

Distribution Grid Optimal Power Flow (D-OPF): Modeling, Analysis, and Benchmarking

Rahul R Jha, *Member, IEEE*, Adedoyin Inaolaji, *Student Member, IEEE*, Biswajit Dipan Biswas, *Student Member, IEEE*, Arun Suresh, *Student Member, IEEE*, Anamika Dubey, *Senior Member, IEEE*, Sumit Paudyal, *Member, IEEE*, Sukumar Kamalasadan, *Senior Member, IEEE*

Abstract—In the power distribution systems, optimal power flow (D-OPF) is formulated as a non-convex and non-linear programming (NLP) problem. Convex relaxation and linear approximation models have been increasingly adopted to achieve computational efficiency for D-OPF. Despite the benefits of scalability and global optimality, each method is based on certain assumptions, performs differently, and may lead to solutions that are physically not meaningful. In this context, this work numerically evaluates the relative performance of second-order cone programming (SOCP), semi-definite programming (SDP), and linear programming (LP) formulations of D-OPF in terms of their feasibility, optimality, and scalability with respect to NLP-based formulations. We also compare the bus injection (in bus voltage and current variables) and branch flow (in active and reactive power flow variables) based on NLP formulations. The performance is evaluated using small (123-node), medium (730-node), and large (2522-node) sized distribution feeders. Case studies, which are backed up by visualization of the analytical models for the solution space to the extent possible, show that (1) the feasibility and exactness of relaxed D-OPF formulations depend upon the problem type, (2) some NLP formulations are computationally more tractable than others, (3) different NLP formulations can converge to different local solutions, and (4) the approximate linear model may underestimate or overestimate the cost function (depending upon the problem type) and may lead to AC-infeasible solutions.

Index Terms—Optimal power flow, power distribution systems, convex relaxation, linear approximation, visualization.

NOMENCLATURE

Sets and Indices

\mathcal{G} Directed graph for distribution system.
 $f(x)$ General problem objective function.
 \mathcal{E} Set of all edges (branches) in \mathcal{G} .
 \mathcal{N} Set of all buses (nodes) in \mathcal{G} .
 \mathcal{N}_C Set of nodes with capacitor banks.
 \mathcal{N}_{DG} Set of nodes with inverter-connected DGs.
 $i \in \mathcal{N}$ $i = \{0, 1, 2, \dots, n\}$ is the node index where node 0 is the substation bus.
 $(i, j) \in \mathcal{E}$ Branch index, also denoted as $i \rightarrow j$.

Parameters

$p_{L,i} + jq_{L,i}$ Complex power demand at node i .
 $q_{cap,i}$ Reactive power supplied by the capacitor connected to the i^{th} node.
 $s_{DG,i}^{rated}$ Rated apparent power capacity for DG connected to node $i \in \mathcal{N}_{DG}$.

$s_{L,i}$ $s_{L,i} = p_{L,i} + jq_{L,i}$ is the complex power demand at node i where $p_{L,i}$ and $q_{L,i}$ are the corresponding active and reactive power demand, respectively.
 V_{min}/V_{max} Minimum/Maximum permissive values of node voltage.
 V_{set}/v_{set} Magnitude/Magnitude-square of the voltage set-point.
 Y_{ij} $Y_{ij} = G_{ij} + jB_{ij}$ is the $(ij)^{th}$ element of network admittance matrix.
 z_{ij} $z_{ij} = r_{ij} + jx_{ij}$ is the impedance of line $i \rightarrow j$.
Variables
 Δv_i $\Delta v_i = |v_i - v_{set}|$ is the deviation between the voltage at node i and a setpoint.
 I_{ij} $I_{ij} = I_{ij} \angle \delta_{ij}$ is the complex line current corresponding to branch (i, j) where, I_{ij} is magnitude and δ_{ij} is corresponding phase angle. In rectangular form, it is written as $I_{ij} = I_{ij}^r + jI_{ij}^i$.
 I_i $I_i = I_i^r + jI_i^i$ is the complex current injected at node i in rectangular form.
 l_{ij} Magnitude-square of the current flowing through branch segment (i, j) .
 $p_{DG,i}$ Active power generated by i^{th} DG.
 $p_{G,0}$ Active power generated by the substation bus.
 $q_{DG,i}$ Reactive power from i^{th} DG.
 $q_{G,0}$ Reactive power generated by the substation bus.
 S_{ij} $S_{ij} = P_{ij} + jQ_{ij}$ is the sending-end complex power flow in branch (i, j) , where, P_{ij} and Q_{ij} are corresponding active and reactive components, respectively.
 V_i $V_i = V_i \angle \theta_i$ is the complex voltage at node i in polar form, and $V_i = V_i^r + jV_i^i$ is complex voltage at node i in rectangular form.
 v_i Magnitude-square of the voltage at node i .
 W $W = VV^H$ is hermitian matrix.
 x General problem variables for objective function $f(x)$.

I. INTRODUCTION

WITH the advancement in smart grid technology and increasing penetrations of distributed generators (DGs), the electric power distribution system is rapidly transforming into an active and bidirectional network. In a centrally managed distribution system, an optimal power flow (OPF) is used for multiple applications related to managing the grid's resources, including, but not limited to, loss minimization, Volt-Var optimization, and effective management of DGs [1], [2]. The literature on OPF formulations from the bulk power grid/transmission systems is not directly applicable to the distribution systems because of radial feeders, high R/X ratio,

This work is supported in part by the U.S. Department of Energy under Contract DE-AC05-76RL01830 and U.S National Science Foundation (NSF) grant ECCS-1944142 awarded to Anamika Dubey, the U.S National Science Foundation (NSF) grant ECCS- 200173 awarded to Sumit Paudyal, and the U.S. National Science Foundation (NSF) grant ECCS-1810174 awarded to Sukumar Kamalasadan.

and large variations in bus voltage magnitudes. Consequently, several researchers have proposed distribution OPF (D-OPF) formulations [3]–[11]. D-OPF models have been based mainly on two power flow formulations: the bus injection model (BIM) and the branch flow model (BFM). Although the bus injection model applies to general radial/mesh feeders, the branch flow model is more suitable for modeling radial distribution feeders. Both BIM and BFM-based D-OPF models in the original form are non-convex and non-linear programming problems (NLP); they are therefore difficult to solve [4].

To address this concern, several relaxed models have been proposed in the literature that tackles the problem of non-convexity either using convex relaxation techniques [5] or using linear approximation methods [12]. For example, a BIM D-OPF formulation is relaxed as a semi-definite program (SDP) by dropping the rank-1 constraint in [6]. Similarly, a BFM D-OPF model can be relaxed by dropping the rank-1 constraint and formulated as an SDP problem. Further, a BFM D-OPF model is relaxed as a second-order cone program (SOCP) by relaxing the quadratic equality constraints in [7]. The SDP and SOCP relaxations proposed in [6], [7] result in convex problems, thus reducing the complexity of the non-linear D-OPF model; however, the conditions for the exactness of the solution obtained from the relaxed models warrant further analysis. Consequently, several researchers have attempted to prove the exactness of relaxed D-OPF models. Sufficient conditions were provided under which the relaxed SOCP and SDP models are exact [8]–[11].

While there has been extensive work on D-OPF, the existing literature lacks a numerical evaluation of the performance of these formulations with different choices of objective functions and network sizes. This is important as the exactness of relaxed models is contingent upon several factors, including the nature of the objective function, physics-based mathematical modeling of the power system, and the solution framework. For example, it has been proved in the existing literature that the SOCP relaxation is exact for the radial distribution feeders under certain conditions [10]. However, the exactness of the SOCP relaxation (for radial feeders) is contingent upon the choice of the objective function. Specifically, SOCP relaxation yields inexact solutions for problem objectives that are not monotonically increasing in power flow variables [13]. Although most D-OPF problems relate to minimizing a cost function of power flow variables, pushing the optimal solution towards the lower bounds of current and voltage variables, there are relevant cases when the optimal solution will require the system variables to operate at their upper bounds. One such case is identifying the maximum photovoltaic (PV) penetration limits for the distribution feeder, also known as PV hosting capacity. Solving this optimization problem using the relaxed D-OPF model (SDP or SOCP) yields AC-infeasible solutions. The resulting solutions from the SOCP model for the PV hosting maximization problem lie inside the second-order cone and not at its boundary [13]. Likewise, for SDP, the solutions are AC-infeasible if the rank-1 constraint is not satisfied [9], [11], [14]. This motivates the evaluation of the existing formulations for AC feasibility using standard distribution feeders for different objective functions and operational scenarios.

Furthermore, given that the original formulation is non-linear, the choice of power flow model in D-OPF may lead to different local optimal solutions. This motivates the need to evaluate D-OPF formulations for solution quality.

The systematic evaluation of the scalability of existing D-OPF formulations at the distribution level is also limited in the literature. This is important because while convex optimization formulations are computationally efficient, not all convex formulations are similar in terms of scalability. For example, SDP relaxation for the BIM is known to not scale well for larger distribution feeders [12], [15]. Similarly, NLP D-OPF models based on specific power flow formulations are found to be more scalable compared to other formulations [16]. Although some recent articles compare D-OPF models, [17]–[19], they are primarily evaluated for small feeders (~ 150 buses) and a simplified problem objective (minimum fuel cost), do not include the visualization for the observations, and do not evaluate the effect of problem type on the exactness of the relaxed and approximate models. Thus, there is a need for a thorough evaluation of the existing D-OPF formulations.

This paper is the first to comprehensively evaluate D-OPF formulations for large feeders with different problem types, along with an intuitive understanding of the observations. Although several theoretical contributions have been made to compare different D-OPF models in the existing literature [8], [20], they derive a limited set of theoretical conditions that do not provide sufficient insights into the implementation details of different D-OPF models. Some questions that are of interest from an implementation point of view include: (1) How scalable are different D-OPF formulations for different D-OPF problems, and how is the scalability affected by the number of decision variables? (2) What are the implications of relaxation and approximation techniques on the solution quality for different problem types, and when is it acceptable to use these techniques? (3) Can we intuitively explain why different D-OPF formulations result in different solutions? To this end, our work complements the existing body of literature through extensive numerical simulations to answer these crucial questions and presents new visualizations of the solution space, when possible, to develop an intuitive understanding of the observations. All D-OPF models are compared for three network-level optimization problems: loss minimization, PV hosting maximization, and voltage deviation minimization. Briefly, the main contributions of this work are listed below.

- A comprehensive numerical evaluation of the relative performance of SOCP, SDP, and linear formulations of D-OPF in terms of their feasibility, optimality, and scalability with respect to NLP-based formulations.
- A novel visualization using a simple two-bus test system that intuitively explains the reason for infeasible solutions from relaxed and approximate D-OPF models for specific problem types. We also visualize problem non-convexity and the possibility of multiple solutions using a notional four-bus radial distribution feeder. These visualizations help explain the crucial observations from the numerical study.
- A comparison of alternate NLP formulations, using branch flow (in active and reactive power flow variables) and bus

injection (in bus voltage and current variables) models for their scalability for a large practical-sized feeder.

Recently, D-OPF models have been extended to solve for discrete and continuous decision variables resulting in mixed-integer nonlinear programming problems (MINLP) [3], [21]. The convex version of the underlying grid model has also been leveraged along with the discrete control of legacy devices, resulting in mixed-integer SOCP (MISOCP) [22]–[24] or mixed-integer SDP (MISDP) [25] versions of D-OPF. Furthermore, multi-period constraints have been managed by solving a multi-period version of the D-OPF problem [26]. These additional considerations add to the complexity of the original nonlinear D-OPF problem. The scope of this work is limited to evaluating the impacts of the nonlinearities resulting from the power flow model on the D-OPF formulations. Thus, the presented analysis mainly considers a deterministic, continuous, single-period D-OPF formulation for the benchmarking study. For thoroughness, we further investigate the effects of integer decision variables on the complexity of the mixed-integer counterparts of the continuous D-OPF formulations.

II. MODELING

We introduce different D-OPF formulations that are used in this benchmarking study. Although there are several versions of D-OPF formulations in the existing literature, we have selected the following formulations for the study: (1) NLP-BIM in Rectangular Coordinate; (2) NLP-BFM in Polar Coordinate; (3) Relaxed SDP-BIM; (4) Relaxed SDP-BFM; (5) Relaxed SOCP-BFM; (6) Linearized BFM (LinDistFlow). These models are selected based on prior evidence of scalability for larger radial distribution feeders [9].

A. Network and Device Models

The distribution system is represented as a connected graph, $\mathcal{G} = (\mathcal{N}, \mathcal{E})$, where \mathcal{N} and \mathcal{E} denote the set of nodes and edges respectively. The edges connect the ordered pair of nodes (i, j) , $\forall i, j \in \mathcal{N}$. Distributed generation (DG) penetration level is defined as the percentage of load nodes that have DGs connected to them. For example, 50% DG penetration implies $|\mathcal{N}_{DG}| = 0.5|\mathcal{N}_L|$, where $|\cdot|$ is the cardinality of a discrete set, \mathcal{N}_{DG} and \mathcal{N}_L denote the set of DG and load nodes, respectively. Also, $(\cdot)^*$ represents the complex-conjugate, $(\cdot)^T$ denotes matrix transpose, and $\mathbf{j} = \sqrt{-1}$.

The distribution lines and transformers are modeled as two-terminal devices with fixed impedance. For each branch, $(i, j) \in \mathcal{E}$, we model the complex impedance as $z_{ij} = r_{ij} + \mathbf{j}x_{ij}$, where, r_{ij} and x_{ij} represent resistance and reactance, respectively. $Y_{ij} = G_{ij} + \mathbf{j}B_{ij}$ denotes the ij^{th} element of the bus admittance matrix. The shunt capacitance of the lines can be included using the Π -model, where shunt capacitance is added on either side of the branch impedance. The loads are modeled as constant power devices. The DGs are modeled as negative loads.

B. Distribution Optimal Power Flow (D-OPF) Formulations

D-OPF problems are formulated as constrained optimization problems consisting of an objective function and a set of grid and operational constraints.

1) *Problem objectives*: Let us assume the problem variables are defined as x . The problem objective is the minimization or maximization of a convex function, $f(x)$. Three different problem objectives are formulated and evaluated in this paper.

- Minimize the total power loss: $\min f(x)$, where, $f(x) = \sum_{(ij) \in \mathcal{E}} l_{ij} r_{ij} = p_{G,0} + \sum_{i \in \mathcal{N}} (p_{DG,i} - p_{L,i})$.
- Maximize the PV hosting capacity: $\max f(x)$, where, $f(x) = \sum_{i \in \mathcal{N}_{DG}} p_{DG,i}$.
- Minimize the voltage deviations with respect to the setpoint voltage: $\min f(x)$, where, $f(x) = \sum_{i \in \mathcal{N}} |v_i - v_{set}|$. This is a non-convex function and is reformulated into a convex function as $f(x) = \sum_{i \in \mathcal{N}} \Delta v_i$, with the inclusion of the following additional constraints, $v_i - v_{set} \leq \Delta v_i$, and $v_{set} - v_i \leq \Delta v_i$.

2) *Operating constraints*: The problem formulation also includes a set of operating constraints as detailed below.

- Node voltage limit: The node voltages need to be maintained with the pre-specified upper and lower limits, V_{min} and V_{max} , where $V_{min} = 0.95$ p.u. and $V_{max} = 1.05$ p.u.
- DG operating limits: The operating points for DG, both $p_{DG,j}$ and $q_{DG,j}$, need to be constrained depending upon the problem formulation. For loss minimization and voltage deviation minimization, we constrain reactive power generation based on the apparent power rating of the DG, $s_{DG,j}^{rated}$, and measured/forecasted value of active power generation, $p_{DG,j}$. For the PV hosting maximization problem, we assume the DGs are operating at unity power factor and we constrain individual DGs power by their maximum active power generation, $p_{DG,j}^{max}$.

3) *D-OPF Models*: It is necessary to model the physics of the network. Depending upon the power flow model, we obtain and describe different versions of D-OPF formulations as follows.

- Non-Linear Programming Bus Injection Model (NLP-BIM): The current-voltage (IV) D-OPF [16] expresses the power flow equations in terms of the current-voltage relationship. Linear network flows are obtained through the current injection method and bilinear terms $(V_i^{re} I_i^{re}, V_i^{im} I_i^{im}, V_i^{re} I_i^{im}, V_i^{im} I_i^{re})$ relate the non-convex constraints. Note that the IV D-OPF formulation has the non-linearities isolated to the bilinear terms which couple variables of a single bus; this makes it scale better compared to other power flow formulations that have non-linearities that couple variables associated with different buses (see Section V). The D-OPF formulation is detailed as follows:

$$\min / \max f(x) \quad (1)$$

Subject to:

Current injection constraints:

$$I_i^{re} = \sum_{j: ij \in \mathcal{E}} V_j^{re} G_{ij} - V_j^{im} B_{ij} \quad (2)$$

$$I_i^{im} = \sum_{j: ij \in \mathcal{E}} V_j^{re} B_{ij} + V_j^{im} G_{ij} \quad (3)$$

Power flow constraints:

$$p_{G,i} = V_i^{re} I_i^{re} + V_i^{im} I_i^{im} + p_{L,i} - p_{DG,i} \quad (4)$$

$$q_{G,i} = V_i^{im} I_i^{re} - V_i^{re} I_i^{im} + q_{L,i} - q_{DG,i} \quad (5)$$

Operating constraints:

$$V_{min}^2 \leq (V_i^{re})^2 + (V_i^{im})^2 \leq V_{max}^2 \quad (6)$$

$$(I_{ij}^{re})^2 + (I_{ij}^{im})^2 \leq (I_{ij}^{rated})^2 \quad (7)$$

where

$$I_{ij}^{re} = -G_{ij}V_i^{re} + B_{ij}V_i^{im} + G_{ij}V_j^{re} - B_{ij}V_j^{im} \quad (8)$$

$$I_{ij}^{im} = -G_{ij}V_i^{im} + B_{ij}V_i^{re} + B_{ij}V_j^{re} + G_{ij}V_j^{im} \quad (9)$$

The reactive power support from DG depends upon the rating of the inverter. For the loss minimization problem, the available reactive power, $q_{DG,j}$ from the inverter is modelled as a box constraint (10),

$$-\sqrt{(s_{DG,j}^{rated})^2 - (p_{DG,j})^2} \leq q_{DG,j} \leq \sqrt{(s_{DG,j}^{rated})^2 - (p_{DG,j})^2} \quad (10)$$

Operating constraints specific to PV hosting maximization:

$$0 \leq p_{DG,j} \leq p_{DG,max} \text{ and } q_{DG,j} = 0 \quad (11)$$

- Non-Linear Programming Branch Flow Model (NLP-BFM): The NLP-BFM [9] formulation for D-OPF problem is detailed below, where power flow constraints are modeled using non-linear branch flow model (BFM). P_{ij} and Q_{ij} are active and reactive power flows in branch (i, j) , respectively.

$$\min / \max f(x) \quad (12)$$

Subject to: Power flow constraints:

$$P_{ij} = \sum_{k: j \rightarrow k} P_{jk} + r_{ij}l_{ij} + p_{L,j} - p_{DG,j} \quad (13)$$

$$Q_{ij} = \sum_{k: j \rightarrow k} Q_{jk} + x_{ij}l_{ij} + q_{L,j} - q_{DG,j} \quad (14)$$

$$v_j = v_i - 2(r_{ij}P_{ij} + x_{ij}Q_{ij}) + (r_{ij}^2 + x_{ij}^2)l_{ij} \quad (15)$$

$$v_i l_{ij} = P_{ij}^2 + Q_{ij}^2 \quad (16)$$

Operating Constraints:

$$V_{min}^2 \leq v_i \leq V_{max}^2 \quad (17)$$

$$l_{ij} \leq (I_{ij}^{rated})^2 \quad (18)$$

Operating constraints specific to loss/voltage deviation: (10). Operating constraints specific to PV maximization: (11).

- Semi-Definite Programming Bus Injection Model (SDP-BIM): D-OPF can be formulated for the power systems represented in bus injection model utilizing the semi-definite programming (SDP) [9]. In this formulation, a matrix variable is defined as $W = VV^H$, where W is a hermitian matrix. This replacement introduces two new constraints $W \succcurlyeq 0$ and $\text{rank}(W) = 1$, denoting respectively that W is a positive semi-definite matrix and the rank of W should be 1. The second constraint ($\text{rank}(W) = 1$) is a non-convex one and by relaxing (i.e., removing) this constraint, the SDP-BIM model is formulated.

The formulation is as follows

$$\min / \max f(x) \quad (19)$$

Subject to: Power flow constraints:

$$p_{G,i} = \sum_{i: i \rightarrow j} \text{Re}\{(W_{ii} - W_{ij})y_{ij}^*\} + p_{L,i} - p_{DG,i} \quad (20)$$

$$q_{G,i} = \sum_{i: i \rightarrow j} \text{Im}\{(W_{ii} - W_{ij})y_{ij}^*\} + q_{L,i} - q_{DG,i} \quad (21)$$

$$W \succeq 0 \quad (22)$$

Operating Constraints:

$$V_{min}^2 \leq W_{ii} \leq V_{max}^2 \quad (23)$$

$$|(W_{ii} - W_{ij})y_{ij}^*|^2 \leq (S_{lm}^{max})^2 \quad (24)$$

Here, the off-diagonal element, W_{ij} , indicates the product of voltages of bus i and bus j i.e. $V_i V_j^H$, that are connected by the branch, (i, j) .

Operating constraints specific to loss/voltage deviation: (10)

. Operating constraints specific to PV maximization: (11).

- Semi-Definite Programming Branch Flow Model (SDP-BFM): The SDP model of D-OPF based on the branch power flow is formulated by utilizing the convexification (28), by relaxing the equality constraint into inequality. Note that $S_{ij} = P_{ij} + \mathbf{j}Q_{ij}$ is sending-end complex power flow in branch (i, j) . The resulting SDP-BFM [9] formulation is as follows:

$$\min / \max f(x) \quad (25)$$

Subject to: Power flow constraints:

$$\sum_{i: i \rightarrow j} (S_{ij} - z_{ij}l_{ij}) = \sum_{k: j \rightarrow k} S_{jk} + s_{L,j} - s_{DG,j} \quad (26)$$

$$v_i - v_j = 2(S_{ij}z_{ij}^* + S_{ij}^*z_{ij}) - z_{ij}l_{ij}z_{ij}^* \quad (27)$$

$$v_i l_{ij} \geq S_{ij}S_{ij}^* \quad (28)$$

Expressing in terms of a positive semi-definite (PSD) matrix, (28) takes the form as follows. Here, upon implementing the SDP relaxation, the rank-1 constraint is then relaxed.

$$\begin{bmatrix} v_i & S_{ij} \\ S_{ij}^* & l_{ij} \end{bmatrix} \succeq 0 \quad (29)$$

$$\text{rank} \begin{bmatrix} v_i & S_{ij} \\ S_{ij}^* & l_{ij} \end{bmatrix} = 1 \quad (30)$$

Operating constraints: (17)-(18). Operating constraints specific to loss/voltage deviation: (10) and PV maximization: (11).

- Second-order Cone Programming (SOCP): The SOCP model [9] for D-OPF is obtained upon relaxing the NLP-BFM model for distribution power flow. Specifically, (16) is first relaxed as an inequality and then expressed as a second-order cone constraint. The resulting relaxed D-OPF formulation is detailed below.

$$\min / \max f(x) \quad (31)$$

Subject to: Power flow constraints: (13)-(15) and

$$\left\| \begin{bmatrix} 2P_{ij} \\ 2Q_{ij} \\ l_{ij} - v_i \end{bmatrix} \right\| \leq l_{ij} + v_i \quad (32)$$

Operating constraints: (17)-(18). Operating constraints are specific to loss/voltage deviation: (10). Operating constraints specific to PV maximization: (11).

- Linear Programming (LP) - LinDistFlow: The LP model for D-OPF is obtained using LinDistFlow power flow model [9]. The resulting D-OPF formulation is detailed below.

$$\min / \max f(x) \quad (33)$$

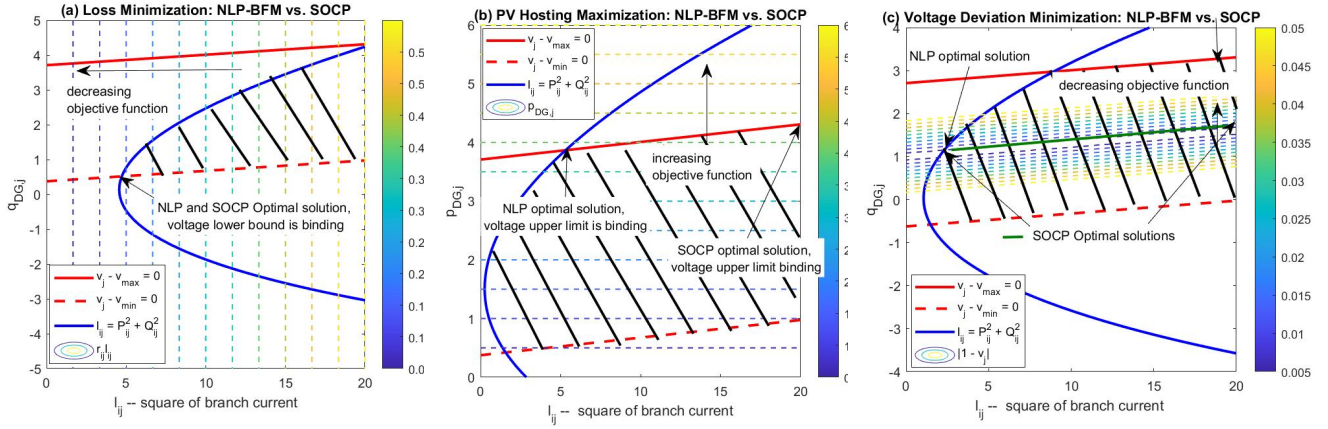


Fig. 1. NLP-BFM vs. SOCP: (a) Loss Minimization; (b) PV Hosting Maximization, and (c) Voltage Deviation Minimization. The feasible space for the NLP problem lies at the boundary of the $l_{ij} = P_{ij}^2 + Q_{ij}^2$ curve, while for the SOCP the feasible space is the shaded area right of the curve.

Subject to: Power flow constraints:

$$P_{ij} = \sum_{k: j \rightarrow k} P_{jk} + p_{L,j} - p_{DG,j} \quad (34)$$

$$Q_{ij} = \sum_{k: j \rightarrow k} Q_{jk} + q_{L,j} - q_{DG,j} \quad (35)$$

$$v_j = v_i - 2(r_{ij}P_{ij} + x_{ij}Q_{ij}) \quad (36)$$

Operating constraints: (17). Operating constraints specific to loss/voltage deviation: (10), and PV maximization: (11).

Discussion (PV Hosting Capacity Maximization): It should be noted that the aforementioned PV hosting capacity problem is a simplified formulation for a complex real-world problem that requires (1) modeling several operation constraints, including constraints on reverse power flow, harmonics, protection, reactive power support, etc., (2) possible non-unity power-factor operation for PVs, and (3) unknown PV locations [27], [28]. A detailed PV hosting problem based on additional criteria can be formulated by adding additional constraints and decision variables to the different D-OPF problem formulations. However, to keep the focus on the computational complexity, feasibility, and optimality of the D-OPF problems, we only considered the PV active power as a control variable. We observed that with the addition of control variables and constraints, the performance of the algorithm follows the same pattern as the base model. This is also corroborated by numerical simulations in Section V.B.

III. VISUALIZATION OF THE SOLUTION SPACE

It has been observed that while convex relaxations are exact for certain problem objectives such as loss minimization and active power minimization, the relaxed model may lead to AC-infeasible¹ solutions for other problem objectives. Our simulation results indicate the same for the following two objectives: (1) PV hosting maximization and (2) voltage deviation minimization. In this section, we attempt to visualize the reason for these results with the help of a simple two-bus system. In the visualization presented, we plot the feasible power flow space specified by the power flow constraints for

¹D-OPF solution is AC-infeasible if it does not satisfy the nonlinear AC power flow constraints.

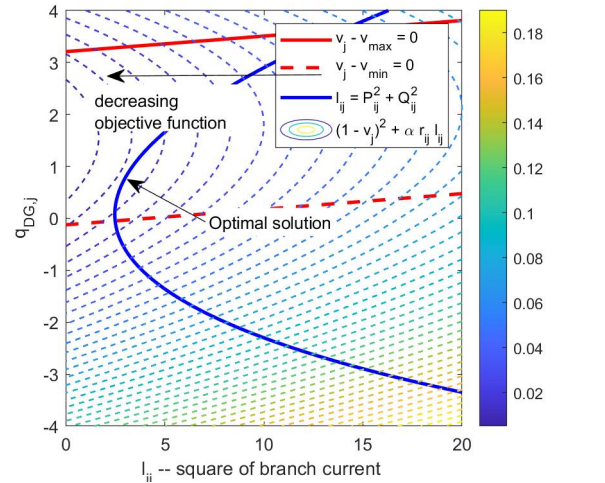


Fig. 2. NLP-BFM vs. SOCP-BFM - Weighted Voltage Deviation and loss Minimization with weight $\alpha = 0.05$. The level sets of the problem objective results in same optimal solutions for both NLP and SOCP problems. The solutions lie at the boundary of the $l_{ij} = P_{ij}^2 + Q_{ij}^2$ curve.

different D-OPF models and the level sets for the problem objective to illustrate the implications of different problem objectives on their ability to reach the optimal and AC-feasible power flow solutions. To this end, we also refer the readers to the existing literature that presents important geometric illustrations for D-OPF models [29]–[31]. Our work corroborates the findings of the existing literature. It extends it to visualize: (1) the nonlinear and relaxed D-OPF model with constraints, (2) the nonlinear and relaxed D-OPF for different problem types, (3) the nonlinear and approximate linear D-OPF (LinDistFlow) for different problem types, and (4) multiple possible solutions in NLP models.

A. Non-linear (BFM/BIM) vs. Relaxed (SOCP/SDP)

This section compares the feasible space for the non-linear and relaxed D-OPF formulations. Our visualization includes constructing the feasible space of the problem defined by the current and voltage constraints and the level sets of the problem objective. Specifically, we compare NLP-BFM and SOCP-BFM formulations for all three problem objectives. We have also validated that the two NLP formulations, NLP-BFM and NLP-BIM, are equivalent. Likewise, SDP-BFM and SOCP-BFM are also validated to be equivalent. Due

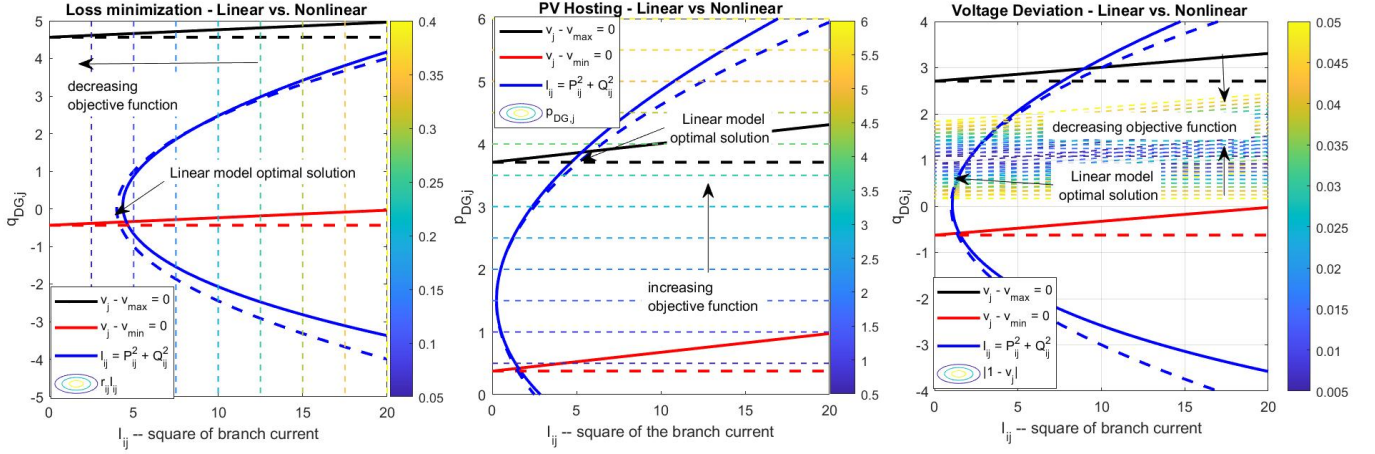


Fig. 3. NLP-BFM (solid lines) vs. LinDistFlow (dashed lines): (a) Loss Minimization, (b) PV Hosting Maximization, and (c) Voltage Deviation Minimization.

to space constraints, the corresponding visualizations are not included. This observation implies that the findings from the visualization in this section also apply to the solutions obtained from NLP-BIM and SDP-BFM models.

For the loss minimization problem, in Fig. 1 (a), we plot the three constraints (to identify the feasible space) and the level sets for the problem objective on $q_{DG,j}$ - l_{ij}^2 2-D plane; $q_{DG,j}$ is the decision variable for the loss minimization problem. As it can be observed, while the feasible power flow space increases for the relaxed SOCP model, the level sets of the problem objective are such that the relaxed SOCP formulation likely results in the same optimal solution as the NLP model. This observation corroborates with the existing literature [9], [10] and the simulation results presented in this paper.

The same analysis is repeated for the PV hosting maximization problem, as shown in Fig. 1 (b). Here, the DG is assumed to operate at a unity power factor, such that $p_{DG,j}$ is the decision variable, while $q_{DG,j}$ is assumed to be not controllable and set to zero. The problem objective is to maximize the active power injection at bus j , i.e., $\max : p_{DG,j}$. The level sets for the problem objective are parallel to $p_{DG,j}$. For this case, while the NLP-BFM model results in the optimal solution at the boundary (of the power flow constraints), the SOCP solution lies in the relaxed problem space. Thus, the relaxed model's solution is inexact for the PV hosting maximization problem. For both models, the upper voltage limits are binding. This is corroborated by [32] where it is proposed that a convex relaxation is guaranteed to be exact for applications with little reverse power flow. It is known, however, that such a condition of slight reverse power flow will typically not be satisfied in a PV hosting maximization problem.

We repeat the analysis for the voltage deviation minimization problem, as shown in Fig. 1 (c). In this case, the problem objective is to minimize $|(V_{set})^2 - v_j|$, where, $V_{set} = V_i = 1$. The control variable is the reactive power dispatch from the inverter, $q_{DG,j}$. We plot the level sets for the objective function and power flow constraints on $q_{DG,j}$ and l_{ij}^2 2-D space. As observed, the level sets are parallel to the lines representing voltage constraints. In the case of a relaxed model, the optimal solution can lie anywhere along with the level set on

the line to the right of the current constraint boundary resulting in the possibility of multiple optimal solutions. Thus, for this objective, as well, the results from the relaxed SOCP model may not be AC-feasible. This is corroborated by [20] where it is stated that AC-feasibility cannot be guaranteed for an objective function that is not monotonic over the feasible set, such as in a voltage deviation minimization problem. However, a weighted problem objective of voltage deviation and loss minimization problem leads to level sets that result in ac-feasible power flow solutions for the relaxed SOCP model (see Fig. 2). Note that the loss minimization objective results in a particular orientation of the level sets (see Fig. 2) that is non-parallel to the voltage constraint lines. Thus, even with a very small weight, the weighted objective function is non-parallel to voltage constraint lines and uniquely intersects them. This results in optimal solutions for the weighted problem for both NLP and SOCP models to lie at the boundary leading to ac-feasible solutions. This is corroborated by [22] where a multi-objective minimization of losses and voltage deviations yielded a tight solution.

These visualization use cases highlight the effect of the objective function on the feasibility of the relaxed SOCP model. Specifically, the level sets of an objective function affect the feasibility of solutions obtained from solving the relaxed OPF problem.

B. Linear vs. Non-linear D-OPF

This section compares the non-linear branch flow D-OPF model against the linear D-OPF model based on LinDistFlow formulation using a two-bus visualization. In Fig.3, we compare the feasible space for all three problem objectives for both linear (LinDistFlow) and non-linear (NLP-BFM) models; the solid and the dashed lines represent the NLP-BFM and the LinDistFlow models, respectively.

First, we observe the current constraint. In the LinDistFlow model, the line losses are ignored in the power balance equations (13)-(14), as well as in the voltage drop equation (15) to obtain the model in (34)-(36). Thus, current equations also do not include the effect of line losses. As a result, the LinDistFlow model underapproximates or overapproximates the current depending upon the region of interest (see Fig. 3). Unlike convex relaxations, which either give a global

solution or at least a lower bound on the optimal solution, approximations can yield solutions that are lower or higher than the global solution [30].

Next, we observe the voltage constraints. The linear model poorly approximates voltage constraints, especially as the branch current increases. Moreover, the linear model underapproximates both overvoltage and undervoltage constraints. Thus, if undervoltage constraints are binding for a given problem, the linear solutions will lead to a violation of feeder voltage limits and undervoltage concerns (see Fig. 3a). Conversely, if the overvoltage constraints are binding, the linear solution will lead to lower voltages than the allowable upper limit at the cost of suboptimal solutions (see Fig. 3a).

It is also necessary to analyze the effects of linearization on the problem objectives. For visualization, the level sets in Fig. 3 are from the non-linear formulation.

For the loss minimization problem shown in Fig. 3a, the linear model could either underapproximate or overapproximate the losses depending upon where the optimal solution lies on the plot. The linear model underapproximates the current and the losses in the lower region. Thus, if the optimal solution lies in the lower region, the actual feeder losses are higher than those estimated by the linear model. While in the upper region, the linear model overapproximates the current and the losses (see Fig. 3a). Thus, if the optimal solution lies in the upper region, the actual feeder losses are lower than those estimated by the linear model. In this particular example, the optimal solution lies in the lower region (Fig. 3a). Thus, the actual feeder losses obtained via the linear model will be higher than those estimated by the linear model. Moreover, the optimal decision variables for the linear problem will differ from the NLP model and lead to higher power losses compared to NLP optimal decisions and possible violations of undervoltage constraints. The linear model underestimates the hosting capacity for the PV hosting maximization problem. Recall that the PV hosting maximization problem is bounded by the upper limit of the voltage. Since the linear model underestimates the upper voltage limit, it results in a conservative estimate of the PV hosting capacity compared to the NLP model (see Fig. 3b). As for the voltage deviation problem, for a voltage reference of 1 p.u., both linear and non-linear models lead to the same optimal solutions as the level sets fall in the region where the linear and non-linear models overlap (see Fig. 3c). This is because the linear model amounts to the least approximation error when the bus voltages are close to 1 p.u. The linear model may lead to different solutions for other voltage setpoints (as observed in our simulation case studies).

C. Non-Convexity and Multiple Solutions

We further visualize the feasible solution space for a four-bus distribution feeder with two DGs in active power control mode. The feasible space admits the power flow solutions that result in bus voltages between 0.95 and 1.05 p.u. (i.e., those satisfying the voltage constraints). Fig. 4 shows the feasible solution space for the example test feeder for NLP, SOCP, and LinDistFlow formulations plotted in the space of decision variables. As observed from Fig. 4a, the feasible space for the NLP-BFM problem is non-convex and can admit

TABLE I TEST SYSTEM DESCRIPTION				
Small-sized Test Feeder - 123-node Test System				
% DG	nodes	total variables	decision variables	number of constraints
0	128	509	0	$382^\ominus, 509^{*\dagger}, 382^\ominus, 512^\circ$
10	128	517	8	$382^\ominus, 509^{*\dagger}, 382^\ominus, 512^\circ$
30	128	534	25	$382^\ominus, 509^{*\dagger}, 382^\ominus, 512^\circ$
50	128	552	43	$382^\ominus, 509^{*\dagger}, 382^\ominus, 512^\circ$
Medium-sized Test Feeder - 730-node Test System				
0	732	2925	0	$2194^\ominus, 2925^{*\dagger}, 2194^\ominus, 2928^\circ$
10	732	2968	43	$2194^\ominus, 2925^{*\dagger}, 2194^\ominus, 2928^\circ$
30	732	3072	147	$2194^\ominus, 2925^{*\dagger}, 2194^\ominus, 2928^\circ$
50	732	3143	218	$2194^\ominus, 2925^{*\dagger}, 2194^\ominus, 2928^\circ$
Large-sized Test Feeder - 2522-node Test System				
0	2522	10085	0	$7564^\ominus, 10085^{*\dagger}, 7564^\ominus, 10088^\circ$
10	2522	10198	113	$7564^\ominus, 10085^{*\dagger}, 7564^\ominus, 10088^\circ$
30	2522	10424	339	$7564^\ominus, 10085^{*\dagger}, 7564^\ominus, 10088^\circ$
50	2522	10650	565	$7564^\ominus, 10085^{*\dagger}, 7564^\ominus, 10088^\circ$

$^\ominus$ LinDistFlow, * NLP-BFM, † SOCP-BFM, $^\circ$ SDP-BFM, $^\circ$ NLP-BIM

multiple possible local optimum solutions. We observe this in our simulation test cases (in Section V-B) for the PV hosting maximization problem. Specifically, for PV hosting maximization, NLP-BIM and NLP-BFM models converge to different local optimum solutions (see Section V-B). We also plot the feasible space for the relaxed SOCP problem for the same four-node test feeder. As shown in Fig. 4b, the SOCP formulation leads to a feasible convex space (without any holes). However, these solutions may be AC-infeasible. The LinDistFlow model leads to a feasible convex space but cuts off the NLP feasible space (see Fig. 4c).

This visualization indicates that the non-convexity of the NLP formulation can lead to multiple possible local optimum solutions, as corroborated in [33]. Also, while relaxed and linearized models avoid non-convexity and multiple possible solutions, they may lead to AC-infeasible solutions (in the case of the relaxed model) or cutoff the NLP optimal solution from the feasible solution space (in the case of the approximate model).

IV. TEST SYSTEM DESCRIPTION

For numerical comparison and benchmarking purposes, the D-OPF formulations detailed in Section II are compared using three example test feeders based on different distribution test feeder models: (1) small-sized feeder: 123-node [34], (2) medium-sized feeder: 730-node [35], and (3) large-sized feeder: 2522-node [34]. The small test feeder, 123-node, is shown in Fig. 5a and is the positive-sequence model for the IEEE 123-bus test system. The 730-node system, shown in Fig. 5b, is generated using the famous 33-node test feeder in [36] with secondary network extensions [35]. Finally, the 2522-node large test feeder, shown in Fig. 5c, is obtained using the IEEE 8500-node test system upon converting it to a positive sequence model and moving the loads to the MV side of the feeder. The feeder characteristics, including the total number of nodes, the total number of variables, the number of decision variables, and the number of constraints (box constraints are excluded), are summarized in Table I.

V. SIMULATION RESULTS

The D-OPF formulations described in Section II are implemented on the test feeders to solve the following three

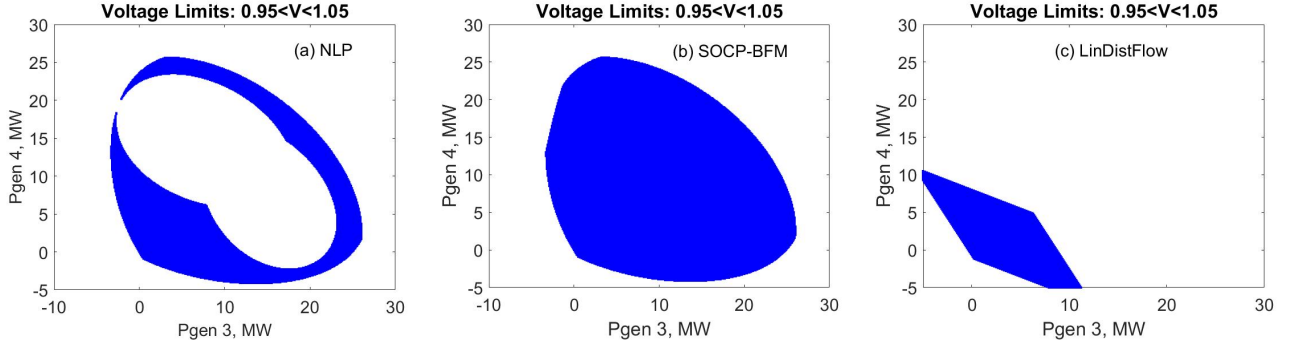


Fig. 4. Four Bus Test Feeder - Feasible space visualization (a,b,c - left to right): (a) NLP-BFM, (b) SOCP-BFM, (c) LinDistFlow. System parameters: $r = 0.55\text{p.u.}$ and $x = 1.33\text{p.u.}$ (for all three branches, 1-2, 2-3 and 2-4), $p_3 = 2\text{MW}$, $q_3 = 0.5\text{MW}$; $p_4 = 1.5\text{MW}$, $q_4 = 0.1\text{MW}$.

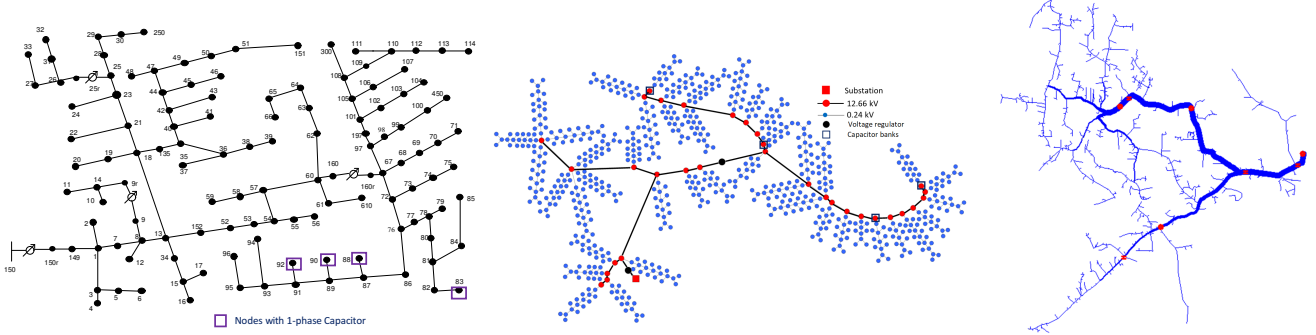


Fig. 5. Test feeders: (a) Small-sized feeder (123 nodes) [34], (b) Medium-sized feeder (730 nodes) [35], (c) Large-sized feeder (2522 nodes) [34].

problem objectives: loss minimization, PV hosting capacity maximization, and voltage deviation minimization. We compare the previously discussed D-OPF formulations: NLP-BIM, NLP-BFM, SDP-BFM, SOCP-BFM, and LinDistFlow. Notice that we do not include the results for SDP-BIM in our case studies as SDP-BIM poses scalability issues and fails to solve even for a small test feeder [12], [15]. The largest network we could solve using the SDP-BIM approach was a 70-node network extracted from the 123-node system shown in Fig. 6a. To validate the results of the SDP-BIM formulation, we also compared and solved the same network using the SDP-BFM, and MATPOWER [37] (which follows an NLP approach). All three approaches yielded the same optimal solution as seen from the voltage profile comparison in Fig. 6b. The computational time for the SDP-BIM was 0.7716s, and the rank of the PSD matrix was 1, which validates the result to be the optimal global solution. When the network size was increased, the solver failed to yield a tight solution using the SDP-BIM approach and instead converged to an optimal point with a rank higher than 1.

The D-OPF formulations are compared for their ability to reach an optimal solution, the feasibility of the relaxed D-OPF models, as well as their solve time and scalability with the increase in the problem size. For both SOCP-BFM and SDP-BFM formulations, the feasibility gap indicates the maximum deviation from achieving equality for the relaxed power flow constraints. We also include OpenDSS [38] validation of the obtained results. Specifically, we measure the substation power flow for each test case upon implementing the decision variable obtained from D-OPF to the OpenDSS models. The D-OPF models are solved using standard computers with up to 16 GB of RAM and 3.41 GHz processors. Depending on the

nature of the D-OPF problems, various solvers (IPOPT, Knitro, Gurobi, CVX, MOSEK, and CPLEX) are used in different modeling languages and toolboxes (e.g., JuMP, MATLAB, YALMIP). The strictest tolerance set in the solvers was $1e^{-8}$.

A. Loss Minimization

The results for loss minimization for the small, medium, and large test feeders are shown in Tables II, III, and IV upon solving the D-OPF problem using four models: NLP-BFM, SOCP-BFM, SDP-BFM, and NLP-BIM.

TABLE II
IEEE 123-BUS SYSTEM, LOSS MINIMIZATION - WITH CAPACITOR ON
AND VOLTAGE REGULATORS (TAPS = 0,0,0)

Total Feeder Losses (kW)					
% DG	W/O Optimization	NLP-BFM	SOCP-BFM	SDP-BFM	NLP-BIM
10	17.8	16.03	16.03	16.06	16.07
30	12.7	10.09	10.08	10.08	10.10
50	7.7	5.19	5.19	5.19	5.20
Compute Time (sec)					
10	NA	21	0.05	0.33	0.29
30	NA	55	0.05	0.33	0.21
50	NA	61	0.03	0.34	0.19
Feasibility Gap (p.u. of MVA×MVA) MVA base = 1					
10	NA	NA	3.97e-6	5.35e-7	NA
30	NA	NA	1.31e-6	2.59e-7	NA
50	NA	NA	3.02e-6	6.52e-7	NA
OpenDSS Validation - Substation Power Flow (kW)					
10	NA	921.00	921.00	921.05	921.06
30	NA	728.50	728.50	728.40	728.43
50	NA	518.62	518.62	518.52	518.53

As it can be observed from Table II, for the small feeder, all four methods converge to the approximately same solution. Both relaxed models, SOCP-BFM and SDP-BFM, solved relatively fast and resulted in a very small feasibility gap,

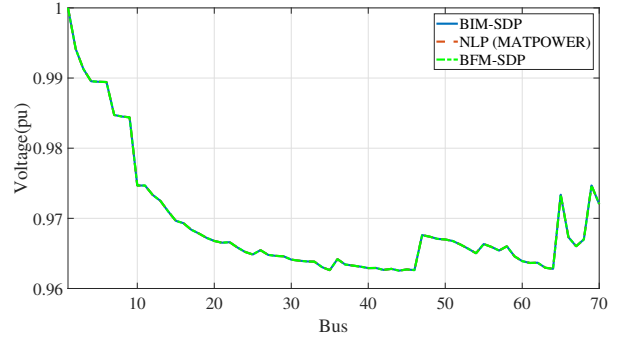
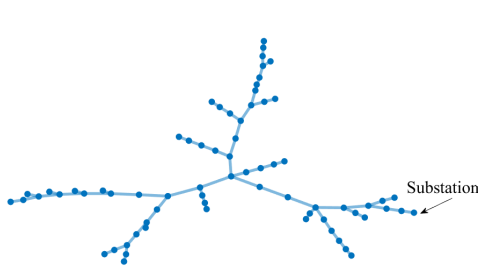


Fig. 6. SDP-BIM simulations: (a) Single line representation of the 70 bus network, and (b) Voltage profile comparison for SDP-BIM, SDP-BFM, and NLP (using MATPOWER).

TABLE III

730-NODE SYSTEM, LOSS MINIMIZATION - WITH CAPACITOR ON AND VOLTAGE REGULATORS (TAPS = 0,0)

Total Feeder Losses (kW)					
% DG	W/O Optimization	NLP-BFM	SOCP-BFM	SDP-BFM	NLP-BIM
10	283.09	273.60	273.60	273.62	273.81
30	163.98	131.0	131.42	131.45	131.50
50	112.6	75.20	75.22	75.24	75.27
Compute Time (sec)					
10	NA	207	0.08	0.55	1.02
30	NA	2485	0.07	0.56	1.42
50	NA	8334	0.10	0.56	1.20
Feasibility Gap (p.u. of MVA×MVA) MVA base = 1					
10	NA	NA	3.52e-6	9.7e-7	NA
30	NA	NA	5.17e-5	5.75e-6	NA
50	NA	NA	6.51e-8	2.65e-6	NA
OpenDSS Validation - Substation Power Flow (MW)					
10	NA	3.62	3.62	3.62	3.62
30	NA	2.59	2.59	2.59	2.59
50	NA	1.93	1.93	1.93	1.93

TABLE IV

2522-NODE SYSTEM, LOSS MINIMIZATION - WITH CAPACITOR ON AND VOLTAGE REGULATORS (TAPS = 0,0,0,0)

Total Feeder Losses (kW)					
DG	W/O Optimization	NLP-BFM	SOCP-BFM	SDP-BFM	NLP-BIM
10	235.9	not solved	224.78	224.76	224.53
30	128.1	not solved	111.47	111.47	111.24
50	63.36	not solved	51.44	51.44	51.22
Compute Time (sec)					
10	NA	NA	0.49	2.12	10.73
30	NA	NA	0.53	2.43	13.89
50	NA	NA	0.64	2.13	21.87
Feasibility Gap (p.u. of MVA×MVA) MVA base = 1					
10	NA	NA	6.19e-4	7.48e-4	NA
30	NA	NA	1.06e-5	1.049e-4	NA
50	NA	NA	3.32e-5	2.71e-4	NA
OpenDSS Validation - Substation Power Flow (MW)					
10	NA	NA	3.15	3.15	3.15
30	NA	NA	2.28	2.28	2.28
50	NA	NA	1.57	1.57	1.57

thus indicating that the relaxed solutions are AC-feasible. The OpenDSS validation of decision variables obtained from all formulations leads to the same substation power flows. All D-OPF models converge within a reasonable time for the small test feeder. Likewise, Table III shows the results for loss minimization for the medium-sized feeder. All four methods approximately converge to the same solution for loss minimization. Both relaxed models, SOCP-BFM and SDP-BFM,

result in a very small feasibility gap, thus implying that the relaxed D-OPF solutions are exact with respect to the original D-OPF problem. Table IV details the results for the loss minimization problem for the large test feeder. For this case, the NLP-BFM model did not converge and posed scalability issues. The rest of the models, including NLP-BIM, converged within a reasonable time (less than a minute) for all cases. Also, both relaxed models reached an optimal and feasible solution with a relatively small feasibility gap. In general, the feasibility gap increases upon increasing the system size. Additional results on voltage profiles and comparison of the other system variables are omitted due to space constraints. The obtained results also corroborate the observations made in Section III via visualization. Specifically, the relaxed SDP and SOCP models are exact and result in an AC-feasible power flow solution for the loss minimization problem (see Fig. 1a). Also, both NLP-BIM and NLP-BFM converge to the same solution. Although multiple locally convergent solutions may exist for the large feeder, the results may be attributed to the same initialization conditions.

The computing time is highest for the NLP-BFM method and increases with the number of decision variables and the feeder size. The time taken by both relaxed models is not significantly affected by the increase in DG penetration levels. However, the solve time slightly increases with the increase in feeder size. The relaxed models converged fastest to the optimal solution. Compared to the NLP-BFM, the NLP-BIM model is much faster and scales well for larger feeders. This result highlights the importance of power flow modeling in scaling the D-OPF models. Note that NLP-BIM uses V-I formulation while NLP-BFM uses P-Q-V variables.

B. PV Hosting Maximization for DG Operating at Unity Power Factor

The results for the PV hosting maximization are discussed next. In the simulation setup, the reactive power dispatch from DGs is assumed to be zero, and net active power dispatch from DGs is maximized to obtain the PV hosting capacity. The DG size is limited to 100 kW each to simulate a realistic case, and the locations are pre-specified. For PV Hosting maximization problem, we compare five D-OPF formulations, including the LinDistFlow model. Recall that the LinDistFlow model is an approximate AC power flow model for radial distribution

TABLE V
IEEE 123-BUS, PV HOSTING, WITH CAPACITOR ON AND VOLTAGE REGULATORS (TAPS = 0,0,0,0) AND MAXIMUM PV RATING 100 kW.

Total PV Hosting Capacity (MW)					
% DG	LinDistFlow	NLP-BFM	SOC-P-BFM	SDP-BFM	NLP-BIM
10	0.80	0.80	0.80	0.80	0.80
30	1.16	1.17	2.50	2.50	1.17
50	1.16	1.18	4.30	4.30	1.18
Compute Time (sec)					
10	0.04	18	0.08	0.26	0.15
30	0.05	155	0.08	0.32	2.3
50	0.06	145	0.06	0.29	3.05
Feasibility Gap (p.u. of MVA×MVA) MVA base = 1					
10	NA	NA	44.09	0.275	NA
30	NA	NA	18.46	1.976	NA
50	NA	NA	57.45	6.169	NA
OpenDSS Validation - Substation Power Flow (kW)					
10	369.41	369.41	369.41	369.37	369.77
30	8.40	0.10	-1229.6	-1229.6	0.01
50	18.35	0.10	-2918.4	-2918.4	0.01

TABLE VI
730-NODE, PV HOSTING - WITH CAPACITOR ON AND VOLTAGE REGULATORS (TAPS = 0,0) AND MAXIMUM PV RATING 100 kW

Total PV Hosting Capacity (MW)					
% DG	LinDistFlow	NLP-BFM	SOC-P-BFM	SDP-BFM	NLP-BIM
10	3.40	3.52	4.30	4.30	3.52
30	3.71	2.52	14.7	14.7	3.83
50	3.71	3.84	21.8	21.8	3.84
Compute Time (sec)					
10	0.07	62.39	0.11	0.52	1.59
30	0.08	136.98	0.11	0.57	4.74
50	0.08	201.36	0.11	0.58	3.95
Feasibility Gap (p.u. of MVA×MVA) MVA base = 1					
10	NA	NA	4.27	2.56	NA
30	NA	NA	19.34	1.86	NA
50	NA	NA	20.10	2.32	NA
OpenDSS Validation - Substation Power Flow (MW)					
10	0.31	0.34	-0.42	-0.42	0.34
30	0.10	1.40	-11.74	-11.74	0.01
50	0.10	0	-20.84	-20.84	0.01

feeders that do not include the effects of line losses on the power flow and voltage drop equations.

Table V shows the results for the 123-node test feeder for cases with 10%, 30%, and 50% DG penetration scenarios. The NLP-BFM and NLP-BIM converge to almost the same solutions for all PV penetration cases. The NLP solutions are also close to the ones obtained using the LinDistFlow model. However, the LinDistFlow model results in a conservative estimate of the PV hosting capacity compared to the NLP model. This observation also corroborates with the visualization in Section III-B (see Fig. 3b). As expected, the solutions obtained using both relaxed models (SOC-P and SDP) do not match with the NLP models and admit a large feasibility gap. This result also corroborates with the observations from Section III for the two-bus visualization case, see Fig. 1b. As previously discussed, the solution for the relaxed D-OPF problem does not lie on the boundary, resulting in an AC-infeasible power flow solution. As for the compute time, NLP-BFM takes the longest to converge; the computation time for the NLP-BFM model also increases with the number of decision variables upon increasing the PV penetration percentage. Other D-OPF models converge relatively fast for all the cases.

Table VI repeats the study for the 730-node medium-sized

TABLE VII
IEEE 123-BUS, PV HOSTING, WITH CAPACITOR ON AND VOLTAGE REGULATORS (TAPS = 0,0,0,0) AND MAXIMUM PV RATING 100 kW AND REACTIVE POWER CONTROL.

Total PV Hosting Capacity (MW)		
% DG	NLP-BFM	NLP-BIM
10	0.80	0.80
30	infeasible	infeasible
50	infeasible	infeasible
Compute Time (sec)		
10	6.81	0.829
30	-	-
50	-	-
OpenDSS Validation - Substation Power Flow (kW)		
10	368.33	376.99
30	-	-
50	-	-

feeder. Compared to the IEEE 123-bus test system, there are two main observations. The first observation is that NLP-BFM takes a very long time to converge to the optimal solution. Secondly, NLP-BFM and NLP-BIM converge to different local solutions for the 30% PV penetration case, indicating that the NLP models can converge to different local optimal solutions. The visualization presented in Section III.C (Fig. 4) explains this observation. Note that both NLP solutions are feasible and locally optimal. Additionally, for this specific case, the PV hosting capacity obtained using the LinDistFlow model lies in between the values obtained using NLP-BIM and NLP-BFM models. Thus, LinDistFlow ends up underestimating the highest of the local optima (or global optimum, if it can be found). As for the relaxed D-OPF models, both SOC-P and SDP models result in a high feasibility gap indicating that the resulting solutions are not tight for the original D-OPF problem, as also discussed in Section III (Figs. 1b and 4b).

Note that NLP-BIM and NLP-BFM did not converge for the large 2522-node test feeder. The non-convergence is due to the inability of the commercial software to solve the resulting large-scale NLP optimization problem, not due to the divergence or the problem of fine-tuning the solver. While both relaxed models, SOC-P and SDP, did converge, they resulted in a very high feasibility gap; thus, the case studies are not further elaborated.

C. PV Hosting Maximization for DG Operating at Non-Unity Power Factor

Further, PV hosting capacity problem is very broad, it varies from a deterministic problem, where the optimal location, size, and effect of voltage control devices are the factors that can be taken into consideration, to a stochastic problem where the uncertainty in the PV power production, load demand, etc are taken into consideration. To show the effect of the addition of control variables and constraints, here we incorporated reactive power control in the NLP-BIM and NLP-BFM as shown in (37). Please note that for simplicity, we have defined this constraints with respect to PV variables which can be generalized for any other DGs with reactive power control. The addition of the reactive power control in the problem formulation will lead to the addition of a nonlinear constraint in the D-OPF as shown below.

$$S_{PV}^2 \geq P_{PV}^2 + Q_{PV}^2 \quad (37)$$

TABLE VIII
2522-NODE, VOLTAGE DEVIATION MINIMIZATION, WITH CAPACITOR ON
AND VOLTAGE REGULATORS (TAPS = 0,0,0,0)

Cost Function					
% DG	LinDistFlow	NLP-BFM	SOC-P-BFM	SDP-BFM	NLP-BIM
10	192.69	not solved	242.62	230.95	231.00
30	82.09	not solved	88.26	85.89	87.70
50	48.79	not solved	33.31	33.08	49.19
Compute Time (sec)					
10	1.38	NA	1.48	2.59	36.88
30	1.59	NA	3.31	5.87	10.64
50	1.53	NA	2.02	6.28	23.34
Feasibility Gap (p.u. of MVA×MVA) MVA base = 1					
10	NA	NA	9.75e-04	0.036	NA
30	NA	NA	34.81	315.15	NA
50	NA	NA	104.71	36700	NA

Note that for the convex D-OPF formulations, i.e., SOCP, SDP, and LinDistFlow, there is a need to approximate the nonlinear constraint into linear constraint using Polyhedral approximation [39]. It has been observed that the addition of linear constraints will not significantly increase the computational complexity of the D-OPF formulation. Thus, we have compared the NLP-BIM and NLP-BFM models for the IEEE 123-node system. Table VII shows the PV hosting comparison of the two NLP models. With the introduction of the reactive power control for the PV hosting problem, the NLP solves only the 10% DG penetration case. It can be observed that despite the introduction of reactive power control, the optimal hosting capacity for the 10% case is 800kW. Further, while validating the solution obtained from the NLP model in OpenDSS, it can be observed that the substation power flow is different for both models. This is because the reactive power support obtained by solving two OPF problems is different for all the PV nodes. Next, for the 30% and 50% test cases, both NLP formulations cannot solve the problem, thus leading to infeasible solutions. Note that for both NLP-BFM and NLP-BIM models, the maximum iterations are set to 1000.

The above simulation results show that the proposed formulation can be easily extended to include additional problem complexities of the PV hosting problem. However, depending upon the nature of the additional constraint, more simplifications or linearizations will be needed to develop scalable optimization models. Developing a scalable model for all constraints is beyond the scope of this work.

D. Voltage Deviation Minimization with Continuous Control Variables

The D-OPF models are compared for the problem objective of minimizing the voltage deviations with respect to a fixed nominal voltage (V_{set}). For all these test cases, we assume the substation voltage, $V_{sub} = 1.05$ p.u. For both small and medium-scale test feeders, both NLP models converge to the same optimal solution. While the relaxed models solve fast, they lead to solutions that are not AC-feasible. The magnitude of the feasibility gap does not show any decipherable pattern. Since there are multiple solutions that the relaxed models can converge on, whether the final solution will be close to the power flow boundary or further away from it can not be determined with certainty (see Fig. 1c). The results for the 2522-node feeder are shown in Table VIII. As it can

be observed, the NLP-BFM model did not converge. NLP-BIM model converged within a reasonable time. Similar to other feeders, the feasibility gap for the relaxed models solved on this large feeder is high for all test cases indicating AC-infeasible solutions. Notice that SOCP and SDP have different feasibility gaps even though they both yield the same solutions. This aligns with our visualization (see Fig. 1c) where SOCP and SDP can have solutions that lie on differing parts of the green line, leading to different feasibility gaps.

For all three test systems, the LinDistFlow model leads to a different cost function, albeit close to the NLP solutions. Note that the visualization in Fig. 3c indicates that the linear and non-linear models overlap in the minimum voltage deviation region. However, this observation is specific to having a substation voltage set to 1.0 p.u. contrary to $V_{sub} = 1.05$ p.u. used here. The linear model ends up underestimating or overestimating the NLP model solutions for different cases. Specifically, for higher DG penetration cases, the linear model ends up mostly overestimating the NLP solutions. We also repeated the case studies with $V_{sub} = 1.0$ p.u. and $V_{set} = 1.0$ p.u. For these case studies, all five models converge to the same optimal solution. Recall the two-bus visualization for this problem objective supports multiple possible solutions for the relaxed models (see Fig. 1c). Thus, relaxed models may converge to AC-infeasible solutions. Simulation cases reveal that while the feasibility gap (for all test cases) is negligible for the $V_{sub} = 1.0$ p.u., setting $V_{sub} = 1.05$ p.u. results in significant feasibility gaps for the relaxed models.

E. Voltage Deviation Minimization with Discrete Control Variables

To show the effect of controlling discrete devices, we further introduce integer variables and solve the voltage deviation problem. To this end, we formulate the mixed-integer programming counterparts of the LP, NLP-BFM, SOCP, SDP, and NLP-BIM models to obtain MILP, MINLP-BFM, MIS-OC, MISDP, MINLP-BIM models respectively. The integer variables represent the ON/OFF control of the capacitor bank switches, where it is assumed that when the capacitor switch is ON, the capacitor is providing its rated reactive power. For comparison, both the substation voltage and the reference voltage are set to 1 pu as shown in Table IX. At 10% DG penetration level, all the mixed-integer counterparts, aside from the MILP formulation, converge to the same optimal solution. Next, for the 30% and 50% test cases, MISOC, MISDP, and MINLP-BIM converge to the same optimal point, but MINLP-BFM converges to a different local optimal point. It should be noted that for the MILP, as the voltage drop due to losses are ignored, it converges at a conservative solution. In terms of the solve time, MILP, MISOC, and MINLP-BIM do not show any significant difference compared to their continuous counterparts. MINLP-BFM and MISDP, on the other hand, have significant computation times compared to their NLP-BFM and SDP counterparts respectively.

F. Discussions and Recommendations

Here, we detail the key observations from the above simulation studies. A summary of these observations is also included in Table X.

TABLE IX
IEEE 123-BUS, VOLTAGE DEVIATION MINIMIZATION FOR THE
MIXED-INTEGER PROBLEM, $V_{sub} = 1.0p.u.$ AND $V_{set} = 1.0p.u.$

Cost Function					
% DG	MILP	MINLP-BFM	MISOCF	MISDP	MINLP-BIM
10	5.41	5.65	5.65	5.65	5.65
30	3.39	3.62	3.56	3.56	3.56
50	1.21	1.67	1.30	1.30	1.29
Compute Time (sec)					
10	0.16	66.68	0.12	9.43	0.28
30	0.18	611.7	0.12	5.47	0.30
50	0.19	1884.98	0.12	4.84	0.33
Feasibility Gap (pu)					
10	NA	NA	$1.33e^{-9}$	$2.85e^{-8}$	NA
30	NA	NA	$1.63e^{-8}$	$2.15e^{-9}$	NA
50	NA	NA	$1.53e^{-7}$	$3.17e^{-9}$	NA
Solver					
-	Cplex	Knitro	Gurobi	CutSDP	Juniper

- For the loss minimization problem, both SOCP-BFM and SDP-BFM relaxations are exact. Both relaxed models reach to same optimal solutions as obtained via NLP models if the original NLP D-OPF problem is feasible. The visualization in Fig. 1a of Section III supports this observation.
- For the loss minimization problem, NLP-BIM, SOCP-BFM, and SDP-BFM models scale well for larger feeders. The solution is obtained within seconds even for the large test feeder with more than 10,000 variables. The NLP-BFM model does not scale well for large problem sizes and does not converge for the large feeder (Tables III and IV).
- For the maximization problem (in this case PV hosting capacity maximization), both SOCP-BFM and SDP-BFM are not exact. That is, there is a significant feasibility gap indicating that the relaxed models do not correspond to a feasible power flow solution. The visualization in Section III, Fig. 1b supports this observation.
- For the maximization problem, we observe that the NLP models, NLP-BIM and NLP-BFM, may lead to different local solutions which are both feasible with respect to the original power flow problem (see Tables V and VI). Visualization in Section III.C Fig. 1b supports this observation.
- Although NLP-BIM shows better scalability with lower computes time, for PV hosting maximization, it runs into convergence issues for the large feeder test case. NLP-BFM does not scale well and does not converge for any of the cases for the large test feeder.
- For the voltage deviation minimization problem, both relaxed D-OPF models, SOCP and SDP, may lead to AC-infeasible power flow solutions. This can also be observed in Fig. 1c. The relaxed models for this problem objective lead to multiple possible solutions. The solution the relaxed model will converge to cannot be determined with certainty and can result in possible AC-infeasible solutions.
- The linear approximation of power flow using LinDistFlow formulation affects the solution quality. It provides a conservative estimate of PV hosting capacity and the violation of operating constraints such as voltage limits. Visualization presented in Section III.B Fig. 3.
- The exactness of the relaxed D-OPF model depends upon the type of the objective function. As noted in the visualization, the slope of the level sets dictates whether the relaxed

model results in a power flow feasible solution. This point is further elaborated in Section III (see Fig. 2).

G. State-of-the-art on Unbalanced D-OPF for Multi-phase Power Distribution Systems

Finally, recognizing that the distribution systems admit three-phase unbalanced operation, we briefly summarize the primary observations for unbalanced D-OPF models based on the existing literature. Due to the mutual coupling among phases and unbalanced loading conditions, the observations based on single-phase D-OPF models do not directly generalize to unbalanced D-OPF models. Primarily, three-phase (unbalanced) D-OPF models admit even stricter conditions on feasibility and are even more challenging to scale. NLP models for unbalanced D-OPF often converge to infeasible or sub-optimal operating points, especially for the large or mid-sized feeder. Recent research in this domain actively looks into scalable algorithms for unbalanced D-OPF that result in a feasible and optimal solution. To this end, there is extensive literature on relaxation and approximation techniques applied to unbalanced D-OPF problem [12], [40]–[44]. Similar to single-phase D-OPF, approximate models can lead to errors [44], [45]. Likewise, the relaxed models have been examined for ac-feasibility. Unfortunately, theoretical results on optimality and feasibility for relaxed models are limited, and there are no theoretical guarantees for exactness on unbalanced D-OPF models. For example, the authors in [12] validated that the relaxed three-phase D-OPF is not exact irrespective of the objective function. Similarly, in [46], authors showed that with the addition of DGs, the BFM-SDP (for loss minimization problem) could not be solved for all test feeders. In [40], it is observed that the SDP relaxation is inexact where the problem objective was to minimize the total electricity cost. As most of the relaxed problems for unbalanced D-OPF were found to be ac-infeasible, several iterative algorithms have also been proposed to obtain ac-feasible solutions [43], [45], [47], [48]. Since unbalanced D-OPF models significantly differ from their balanced counterparts, a separate comparative study is needed to understand the behavior of these models fully.

VI. CONCLUSION

This paper extensively evaluates the performance of a suite of non-linear models, linear approximations, and convex relaxations of the D-OPF formulation regarding feasibility, optimality, and scalability. The main observations are: (1) the feasibility of relaxed D-OPF formulations depends upon the problem type, (2) some NLP formulations are computationally more tractable than others, (3) different NLP formulations can converge to different local solutions, and (4) LinDistFlow model may underestimate or overestimate the cost function (depending upon the problem type) and may lead to AC-infeasible solutions. We provide the readers with a comprehensive implementation-centric understanding of different D-OPF models, including the limitations of each approach for common classes of D-OPF problems. Case studies are also backed up by visualization to better understand the observations. This work attempts to fill the lacuna in the

TABLE X
SUMMARY OF OBSERVATIONS

Loss Minimization						
D-OPF Model	Feasibility	Optimality	Accuracy	Scalability	Usability	Comments
LinDistFlow	NA	NA	NA	NA	NA	None
NLP-BFM	May not be feasible	Global/Local optimal	Very accurate	Does not scale	Medium	Slow but accurate
NLP-BIM	Feasible	Global/Local optimal	Very accurate	Scalable	High	Fast and accurate
SOC-P-BFM	Feasible	Global optimal	Very accurate ¹	Scalable	High	Very Fast and accurate
SDP-BFM	Feasible	Global optimal	Very accurate ²	Scalable	High	Very Fast and accurate
PV Hosting Maximization						
D-OPF Model	Feasibility	Optimality	Accuracy	Scalability	Usability	Comments
LinDistFlow	Feasible	Local optimal	Not accurate but close	Scalable	Medium	Fast, Not accurate but close
NLP-BFM	May not be feasible	Global/Local optimal	Very accurate	Does not scale	Medium	Slow but accurate
NLP-BIM	May not be feasible	Global/Local optimal	Very accurate	Does not scale	Medium	Fast if converges
SOC-P-BFM	Feasible	Global optimal	Not accurate	Scalable	Low	Fast, not accurate
SDP-BFM	Feasible	Global optimal	Not accurate	Scalable	Low	Fast, not accurate
Voltage Deviation Minimization						
D-OPF Model	Feasibility	Optimality	Accuracy	Scalability	Usability	Comments
LinDistFlow	Feasible	Local optimal	Not accurate but close	Scalable	Medium	Fast, Not accurate but close
NLP-BFM	May not be feasible	Global/Local optimal	Very Accurate	Does not scale	Medium	Slow but accurate
NLP-BIM	Feasible	Global/Local optimal	Very Accurate	Scalable	High	Fast and accurate
SOC-P-BFM	Feasible	Global optimal	May not be accurate	Scalable	Low	Fast, May not be accurate
SDP-BFM	Feasible	Global/Local optimal	May not be accurate	Scalable	Low	Fast, May not be accurate

Feasibility indicates implementation capabilities. Optimality is with respect to original problem's global optimum. Accuracy indicates AC-feasibility.
Usability Score: High \Rightarrow feasible, fast and accurate, Medium \Rightarrow may not be fast or accurate, Low \Rightarrow infeasible
NA: Not Applicable, 1, 2: certain network conditions need to hold.

area of modeling, analysis, and benchmarking the performance of D-OPF models and serve as a guide/reference point for researchers and utilities in making informed decisions on these well-known formulations. As part of future work, we will model, analyze and benchmark power flow and D-OPF formulations on unbalanced multi-phase networks.

REFERENCES

- [1] W. Sheng, K. Liu, and S. Cheng, "Optimal Power Flow Algorithm and Analysis in Distribution System Considering Distributed Generation," *IET Generation, Transmission and Distribution*, vol. 8, pp. 261–272, February 2014.
- [2] M. Huneault and F. D. Galiana, "A Survey of the Optimal Power Flow Literature," *IEEE Trans. Power Systems*, vol. 6, pp. 762–770, May 1991.
- [3] S. Paudyal, C. A. Cañizares, and K. Bhattacharya, "Optimal Operation of Distribution Feeders in Smart Grids," *IEEE Trans. on Ind. Electron.*, vol. 58, pp. 4495–4503, Oct. 2011.
- [4] S. Paudyal, C. A. Cañizares, and K. Bhattacharya, "Three-phase Distribution OPF in Smart Grids: Optimality versus Computational Burden," in *Proc. IEEE PES International Conference and Exhibition on Innovative Smart Grid Technologies*, pp. 1–7, Dec 2011.
- [5] S. Low, "Convex Relaxation of Optimal Power Flow -Part I: Formulations and Equivalence," *IEEE Transactions on Control of Network Systems*, vol. 1, pp. 15–27, Mar. 2014.
- [6] X. Bai and H. Wei, "Semi-Definite Programming-based Method for Security-Constrained unit Commitment with Operational and Optimal Power Flow Constraints," *IET Generation, Transmission Distribution*, vol. 3, pp. 182–197, February 2009.
- [7] R. A. Jabr, "Radial distribution load flow using conic programming," *IEEE Trans. on Power Systems*, vol. 21, pp. 1458–1459, Aug 2006.
- [8] D. K. Molzahn and I. A. Hiskens, "Convex Relaxations of Optimal Power Flow Problems: An Illustrative Example," *IEEE Transactions on Circuits and Systems I: Regular Papers*, vol. 63, pp. 650–660, May 2016.
- [9] M. Farivar and S. H. Low, "Branch Flow Model: Relaxations and Convexification: Part I," *IEEE Transactions on Power Systems*, vol. 28, pp. 2554–2564, Aug 2013.
- [10] S. H. Low, "Convex Relaxation of Optimal Power Flow Part II: Exactness," *IEEE Transactions on Control of Network Systems*, vol. 1, pp. 177–189, June 2014.
- [11] L. Gan, N. Li, U. Topcu, and S. H. Low, "Exact Convex Relaxation of Optimal Power Flow in Radial Networks," *IEEE Transactions on Automatic Control*, vol. 60, pp. 72–87, Jan 2015.
- [12] L. Gan and S. H. Low, "Convex relaxations and linear approximation for optimal power flow in multiphase radial networks," in *2014 Power Systems Computation Conference*, pp. 1–9, IEEE, 2014.
- [13] R. R. Jha and A. Dubey, "Exact Distribution Optimal Power Flow (D-OPF) Model using Convex Iteration Technique," in *2019 IEEE Power Energy Society General Meeting (PESGM)*, pp. 1–5, Aug 2019.
- [14] B. D. Biswas and S. Kamalasadan, "Alternative SDP Relaxed Optimal Power Flow Formulation for Radial Distribution Networks," in *2022 IEEE International Conference on Power Electronics, Smart Grid, and Renewable Energy (PESGRE)*, pp. 1–6, 2022.
- [15] J. Lavaei and S. H. Low, "Zero Duality Gap in Optimal Power Flow Problem," *IEEE Trans. on Power Systems*, vol. 27, pp. 92–107, 2012.
- [16] M. B. Cain, R. P. O'Neill, A. Castillo, et al., "History of Optimal Power Flow and Formulations," *Federal Energy Regulatory Commission*, vol. 1, pp. 1–36, 2012.
- [17] A. Inaolaji, A. Savasci, S. Paudyal, and S. Kamalasadan, "Accuracy of Phase-Decoupled and Phase-Coupled Distribution Grid Power Flow Models," in *Proc. IEEE Power Energy Society Innovative Smart Grid Technologies Conference (ISGT)*, pp. 1–5, 2021.
- [18] M. Vanin, H. Ergun, R. D'hulst, and D. Van Hertem, "Comparison of Linear and Conic Power Flow Formulations for Unbalanced Low Voltage Network Optimization," *Electric Power Systems Research*, vol. 189, p. 106699, 2020.
- [19] D. M. Fobes, S. Claeys, F. Geth, and C. Coffrin, "PowerModelsDistribution.jl: An open-source framework for exploring distribution power flow formulations," *Electric Power Systems Research*, vol. 189, 2020.
- [20] Q. Li and V. Vittal, "Non-iterative Enhanced SDP Relaxations for Optimal Scheduling of Distributed Energy Storage in Distribution Systems," *IEEE Trans. on Power Systems*, vol. 32, no. 3, pp. 1721–1732, 2016.
- [21] Z. Wang, J. Wang, B. Chen, M. M. Begovic, and Y. He, "Mpc-based voltage/var optimization for distribution circuits with distributed generators and exponential load models," *IEEE Transactions on Smart Grid*, vol. 5, no. 5, pp. 2412–2420, 2014.
- [22] S. R. Shukla, S. Paudyal, and M. R. Almassalkhi, "Efficient distribution system optimal power flow with discrete control of load tap changers," *IEEE Trans. on Power Systems*, vol. 34, no. 4, pp. 2970–2979, 2019.
- [23] W. Wu, Z. Tian, and B. Zhang, "An exact linearization method for oltc of transformer in branch flow model," *IEEE Transactions on Power Systems*, vol. 32, no. 3, pp. 2475–2476, 2017.
- [24] R. A. Jabr, R. Singh, and B. C. Pal, "Minimum loss network reconfiguration using mixed-integer convex programming," *IEEE Transactions on Power Systems*, vol. 27, pp. 1106–1115, May 2012.
- [25] I. Alsaleh and L. Fan, "Multi-time co-optimization of voltage regulators and photovoltaics in unbalanced distribution systems," *IEEE Transactions on Sustainable Energy*, pp. 1–1, 2020.
- [26] R. Zafar, J. Ravishankar, J. E. Fletcher, and H. R. Pota, "Optimal dispatch of battery energy storage system using convex relaxations in unbalanced distribution grids," *IEEE Transactions on Industrial Informatics*, vol. 16, no. 1, pp. 97–108, 2019.

- [27] A. Dubey and S. Santoso, "On estimation and sensitivity analysis of distribution circuit's photovoltaic hosting capacity," *IEEE Transactions on Power Systems*, vol. 32, no. 4, pp. 2779–2789, 2017.
 - [28] S. Jothibasu, S. Santoso, and A. Dubey, "Optimization methods for evaluating pv hosting capacity of distribution circuits," in *2019 IEEE 46th Photovoltaic Specialists Conference (PVSC)*, pp. 0887–0891, 2019.
 - [29] B. Zhang, A. Y. Lam, A. D. Domínguez-García, and D. Tse, "An optimal and distributed method for voltage regulation in power distribution systems," *IEEE Transactions on Power Systems*, vol. 30, no. 4, pp. 1714–1726, 2015.
 - [30] L. Gan, N. Li, U. Topcu, and S. H. Low, "Exact convex relaxation of optimal power flow in radial networks," *IEEE Transactions on Automatic Control*, vol. 60, no. 1, pp. 72–87, 2014.
 - [31] S. Bose, S. H. Low, T. Teeraratkul, and B. Hassibi, "Equivalent relaxations of optimal power flow," *IEEE Transactions on Automatic Control*, vol. 60, no. 3, pp. 729–742, 2015.
 - [32] S. Huang, Q. Wu, J. Wang, and H. Zhao, "A sufficient condition on convex relaxation of ac optimal power flow in distribution networks," *IEEE Transactions on Power Systems*, vol. 32, no. 2, pp. 1359–1368, 2016.
 - [33] W. A. Bukhsh, A. Grothey, K. I. McKinnon, and P. A. Trodden, "Local solutions of the optimal power flow problem," *IEEE Transactions on Power Systems*, vol. 28, no. 4, pp. 4780–4788, 2013.
 - [34] "Distribution Test Feeders," <http://ewh.ieee.org/soc/pes/dsacom/testfeeders/>, IEEE PES.
 - [35] H. K. Vemprala, M. A. I. Khan, and S. Paudyal, "Open-source Poly-phase Distribution System Power Flow Analysis Tool (DxFlow)," in *Proc. IEEE Inter. Conf. on Electro Information Technology (EIT)*, 2019.
 - [36] M. Baran and F. Wu, "Network Reconfiguration in Distribution Systems for Loss Reduction and Load Balancing," *IEEE Transactions on Power Delivery*, vol. 4, no. 2, pp. 1401–1407, 1989.
 - [37] R. D. Zimmerman and C. E. Murillo-Sánchez, "Matpower 6.0 user's manual," *Power Systems Engineering Research Center*, vol. 9, 2016.
 - [38] R. C. Dugan and T. E. McDermott, "An Open Source Platform for Collaborating on Smart Grid Research," in *2011 IEEE Power and Energy Society General Meeting*, pp. 1–7, IEEE, 2011.
 - [39] R. A. Jabr, "Linear decision rules for control of reactive power by distributed photovoltaic generators," *IEEE Transactions on Power Systems*, vol. 33, no. 2, pp. 2165–2174, 2018.
 - [40] W. Wang and N. Yu, "Chordal conversion based convex iteration algorithm for three-phase optimal power flow problems," *IEEE Transactions on Power Systems*, vol. 33, no. 2, pp. 1603–1613, 2017.
 - [41] A. S. Zamzam, N. D. Sidiropoulos, and E. Dall'Anese, "Beyond relaxation and newton-raphson: Solving ac opf for multi-phase systems with renewables," *IEEE Transactions on Smart Grid*, vol. 9, no. 5, pp. 3966–3975, 2016.
 - [42] E. Dall'Anese, H. Zhu, and G. B. Giannakis, "Distributed optimal power flow for smart microgrids," *IEEE Transactions on Smart Grid*, vol. 4, no. 3, pp. 1464–1475, 2013.
 - [43] S. S. Guggilam, E. Dall'Anese, Y. C. Chen, S. V. Dhople, and G. B. Giannakis, "Scalable optimization methods for distribution networks with high pv integration," *IEEE Transactions on Smart Grid*, vol. 7, no. 4, pp. 2061–2070, 2016.
 - [44] A. Bernstein and E. Dall'Anese, "Linear power-flow models in multi-phase distribution networks," in *2017 IEEE PES Innovative Smart Grid Technologies Conference Europe (ISGT-Europe)*, pp. 1–6, IEEE, 2017.
 - [45] S. Bolognani and F. Dörfler, "Fast power system analysis via implicit linearization of the power flow manifold," in *2015 53rd Annual Allerton Conference on Communication, Control, and Computing (Allerton)*, pp. 402–409, IEEE, 2015.
 - [46] Z. Wang, D. S. Kirschen, and B. Zhang, "Accurate semidefinite programming models for optimal power flow in distribution systems," *arXiv preprint arXiv:1711.07853*, 2017.
 - [47] A. S. Zamzam, N. D. Sidiropoulos, and E. Dall'Anese, "Beyond relaxation and newton-raphson: Solving ac opf for multi-phase systems with renewables," *IEEE Transactions on Smart Grid*, vol. 9, no. 5, pp. 3966–3975, 2018.
 - [48] R. R. Jha and A. Dubey, "Network-level optimization for unbalanced power distribution system: Approximation and relaxation," *IEEE Transactions on Power Systems*, vol. 36, no. 5, pp. 4126–4139, 2021.
- Rahul Ranjan Jha** (M'16) received the B.Tech degree from the School of Engineering, Cusat, Kerala, India, in 2012, and the M.Tech degree from the Electrical Engineering Department, IIT Kanpur, Kanpur, India, in 2015 and a Ph.D. degree in Electrical Engineering from Washington State University, Pullman, WA in 2020. He is currently a General Engineer at the ComEd. His current research interests include optimal power flow, centralized and distributed algorithms for improving the efficiency of the distribution network with grid-edge devices.
- Adedoyin Inaolaji** (S'19) received a B.Eng. degree in Electrical and Electronics Engineering from Covenant University, Ota, Nigeria, in 2014, and an M.S. degree in Electrical Engineering from the Department of Electrical and Computer Engineering, Florida International University (FIU), Miami, FL, USA in 2022, where she is currently working toward the Ph.D. degree in Electrical Engineering. Her research interests include distribution grid modeling, analysis, and optimization techniques.
- Biswajit Dipan Biswas** (S'19) received his B.Eng. degree in Electrical and Electronics Engineering from Bangladesh University of Engineering and Technology, Bangladesh, in 2013. He worked as an Operation Engineer at KEPCO-KPS in Bangladesh from 2013 to 2017. He is currently working as a PhD candidate in Electrical Engineering at UNC Charlotte. His current research interests include convex optimization problem in power distribution systems with high penetration with distributed energy resources.
- Arun Suresh** (S'12) received the B.Tech degree in electrical engineering from Mahatma Gandhi University, India, in 2012 and M.Tech degree in electrical engineering from Kerala University, India, in 2015. He completed his Ph.D. degree in electrical engineering from the University of North Carolina, Charlotte, NC, USA in 2021. He is currently working as Consultant at Hitachi Energy, Raleigh, USA. His research interests include Power system stability and control, Smart grid, and integration of renewable energy in power systems.
- Anamika Dubey** (SM'21) received her Ph.D. degree in Electrical and Computer Engineering from the University of Texas at Austin in Dec 2015. She is currently Huie-Rogers Endowed Chair Associate Professor of Electrical Engineering in the School of EECS at Washington State University (WSU), Pullman. She also holds a joint appointment as a Research Scientist at the Pacific Northwest National Laboratory (PNNL). Her research focuses on the optimization and control of large-scale electric power distribution systems for improved efficiency, flexibility, and resilience. Her expertise is in modeling, analyzing, and operating active power distribution systems with massive penetrations of controllable grid-edge resources (including DERs, EVs, and GEBs).
- Sumit Paudyal** (M'12) received the B.E. degree from Tribhuvan University, Nepal in 2003, the M.Sc. degree from the University of Saskatchewan, Saskatoon, Canada, in 2008, and the Ph.D. degree from the University of Waterloo, Waterloo, Canada, in 2012, all in electrical engineering. He was a faculty member at Michigan Technological University, Houghton, MI, USA from 2012 to 2019. Since 2019, he is an Associate Professor in the Department of Electrical and Computer Engineering at Florida International University, Miami, FL, USA. His research interests include distribution grid modeling, dynamic studies, and optimization techniques in power systems.
- Sukumar Kamalasadan** (SM'17) received the B.Tech. degree in electrical and electronics engineering from the University of Calicut, India, in 1991, the M.Eng. degree in electrical power systems management from the Asian Institute of Technology, Bangkok, Thailand, in 1999, and the Ph.D. degree in electrical engineering from The University of Toledo, Toledo, OH, USA, in 2004. He is a Professor in the Department of Electrical and Computer Engineering at the University of North Carolina at Charlotte, Charlotte, NC, USA. His research interests include intelligent and autonomous control, power systems dynamics, stability and control, smart grid, microgrid, and real-time optimization and control of power system. He is a recipient of the National Science Foundation (NSF) CAREER Award and IEEE Best Paper Awards. He is the chair of IEEE Power and Energy Society (PES) Power and Energy Education Committee, member of 2022 IEEE PES Leadership Team and Council member of IEEE Industry Application Society (IAS).